Journal of Power Sources 284 (2015) 416–427

Contents lists available at ScienceDirect

Journal of Power Sources

journal homepage: www.elsevier.com/locate/jpowsour

Degradation of the solid electrolyte interphase induced by the deposition of manganese ions

Hosop Shin [a], Jonghyun Park [a, 1], Ann Marie Sastry [b], Wei Lu [a, *]

[a] Department of Mechanical Engineering, University of Michigan, Ann Arbor, MI 48109, USA
[b] Sakti3, Ann Arbor, MI 48108, USA

HIGHLIGHTS

- Characterized SEI changes that occur in the presence of dissolved Mn ions.
- Identified the MnF_2 specie resulting from the interaction between SEI and Mn ions.
- Demonstrated the deposition mechanism of Mn compound at the SEI/graphite interface.
- Revealed the spatial distribution of Mn deposited at the SEI/graphite interface.

GRAPHICAL ABSTRACT

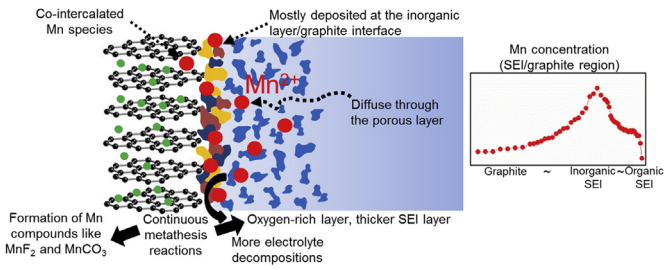

ARTICLE INFO

Article history:
Received 9 January 2015
Received in revised form
4 March 2015
Accepted 5 March 2015
Available online 6 March 2015

Keywords:
Li-ion battery
Solid electrolyte interphase
Mn dissolution
Mn deposition
Capacity fade
Ion-exchange mechanism

ABSTRACT

The deposition of manganese ions dissolved from the cathode onto the interface between the solid electrolyte interphase (SEI) and graphite causes severe capacity fading in manganese oxide-based cells. The evolution of the SEI layer containing these Mn compounds and the corresponding instability of the layer are thoroughly investigated by artificially introducing soluble Mn ions into a 1 mol L^{-1} $LiPF_6$ electrolyte solution. Deposition of dissolved Mn ions induces an oxygen-rich SEI layer that results from increased electrolyte decomposition, accelerating SEI growth. The spatial distribution of Mn shows that dissolved Mn ions diffuse through the porous layer and are deposited mostly at the inorganic layer/graphite interface. The Mn compound deposited on the anode, identified as MnF_2, originates from a metathesis reaction between LiF and dissolved Mn ion. It is confirmed that ion-exchange reaction occurs in the inorganic layer, converting SEI species to Mn compounds. Some of the Mn is observed inside the graphite; this may cause surface structural disordering in the graphite, limiting lithium-ion intercalation. The continuous reaction that occurs at the inorganic layer/graphite interfacial regions and the modification of the original SEI layer in the presence of Mn ions are critically related to capacity fade and impedance rise currently plaguing Li-ion cells.

1. Introduction

The capacity and power fading of lithium-ion (Li-ion) batteries are complicated processes that are very challenging to understand and resolve, especially at elevated temperatures [1–6]. Although the mechanisms responsible for the degradation of Li-ion batteries cannot be simplified and explained by one or two phenomena, the

* Corresponding author.
E-mail address: weilu@umich.edu (W. Lu).
[1] Current address: Department of Mechanical and Aerospace Engineering, Missouri University of Science and Technology, Rolla, MO 65409, USA.

http://dx.doi.org/10.1016/j.jpowsour.2015.03.039
0378-7753/

dissolution of the active materials and the instability of the solid electrolyte interphase (SEI) are two of the key phenomena responsible for the degradation. These two phenomena, in particular, cannot be considered independent at elevated temperatures, since a significant amount of the ions dissolved at elevated temperatures move to the anode side and modify the SEI layer. Consequently, transition metal dissolution from the cathode materials not only influences the reversible capacity of the positive electrode, it also influences the reversible capacity of the negative electrode.

The dissolution of active materials from the cathode side clearly causes the loss of usable materials from the positive electrode. These dissolved transition-metal ions subsequently re-deposit on the positive electrode, forming an electrically insulating layer of oxides and fluorides [4,7]. Moreover, the dissolved ions diffuse to the negative electrode, where they are deposited, influencing both the chemical degradation of the SEI layer and the self-discharge of the lithiated anode [8,9]. These phenomena are especially important for manganese-based electrodes, such as $LiMn_2O_4$, $LiMnO_2$, $Li_{1+x}Mn_2O_4$, and $Li_{1.05}(Ni_{1/3}Co_{1/3}Mn_{1/3})_{0.95}O_2$, since the manganese-based oxides are more vulnerable to dissolution in the electrolyte than other cathode materials, especially at elevated temperatures [10]. It has been also reported that the amount of Mn deposited is significantly greater than that of other transition metals, such as Ni and Co [11]. Thus, in manganese-based cells, a considerable amount of Mn ions is expected to be continuously dissolved and deposited during prolonged storage/cycling at elevated temperatures.

The instability of the SEI on the anode is severe especially at elevated temperatures; two factors, i.e., temperature and dissolved Mn ions, considerably contribute to degradation of the SEI layer [2,3,8,9]. Fig. 1 shows a simple schematic of the degradation of the SEI on the graphite that occurs at elevated temperatures. As shown in the figure, two different mechanisms are associated with the degradation of the SEI: (1) Elevated temperatures directly induce the dissolution, breakdown, and conversion of the SEI layer, which make the original SEI layer to be a defective layer [1–3]. This defective layer causes the consumption of cyclable lithium ions and additional decomposition of the electrolyte to reform the layer, resulting in the growth of the SEI layer. (2) The dissolved Mn ions also induce side reactions associated with the deposition of the Mn ions, resulting in a defective layer [8,9,12]. During the deposition process, Mn ions can interact with the chemical species in the SEI layer, and deposited Mn compounds can promote a catalytic reaction that results in more decomposition of the electrolyte. In addition, the deposition of the dissolved Mn ions can make lithium ions in the lithiated graphite to deintercalate during the reduction process [8]. Thus, degradation of the SEI layer proceeds in the presence of the dissolved Mn ions, reducing capacity and power of a Li-ion battery. At elevated temperatures, these two phenomena simultaneously occur and are coupled to each other, which make understanding the mechanism of SEI layer degradation more complex.

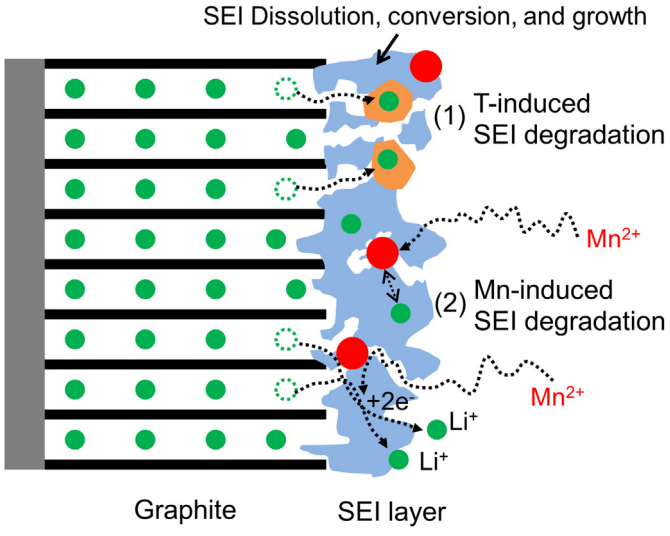

Fig. 1. A schematic description of the SEI instability that occurs in cycled or stored Li-ion batteries at elevated temperatures.

To simplify the problem and get a better insight into the influence of Mn deposition on capacity fade, several studies have been conducted by artificially introducing soluble Mn ions into the electrolytes. Either a defined amount of the manganese perchlorate [$Mn(ClO_4)_2$] has been dissolved in $LiClO_4$-based electrolytes or the anodic dissolution of Mn metal has been carried out using electrolysis [9,12–15]. These previous studies provide limited information that is only applicable to $LiClO_4$-based electrolyte systems because, in each case, a lithium salt ($LiClO_4$) was used as the electrolyte. Moreover, the presence of hydrofluoric acid (HF), which is an important reason for Mn dissolution in $LiPF_6$-based electrolytes, has been ignored in $LiClO_4$-based electrolyte systems. A recent study tried to mimic the conditions in $LiPF_6$-based commercial cells by immersing $LiMn_2O_4$ powder in the electrolyte at the high temperature for several days [16]. However, this preparation could cause the degradation of the electrolyte during the storage, producing byproducts such as HF, PO_3F^{2-}, and $PO_2F_2^-$ in the electrolyte [17]. In addition, it is difficult to achieve the desired amount of dissolved Mn ions in the electrolyte.

So far, a number of efforts have been made to understand the influence of Mn deposition on anode performance, the interaction mechanism between dissolved Mn ions and the anode/electrolyte interface, and the oxidation state of the deposited Mn. The deterioration of anode performance induced by Mn deposition has been clearly observed with increased reduction current and interfacial impedance [12–16,18]. However, earlier studies have shown conflicting results about the mechanism responsible for Mn compound deposition and the oxidation state of the deposited Mn compound. This makes it difficult to have a clear understanding of what happens at the anode/electrolyte interface as a result of the deposition of Mn ions. It was initially proposed that the dissolved Mn ions could be reduced electrochemically by the low potential, based on the known standard redox potential of Mn/Mn^{2+} (1.87 V vs. Li/Li^+) [12]. Another hypothesis was that the reduction of the Mn ions on the anode surface occurs chemically, via the chemical activity of the lithiated graphite [18]. Another possibility has recently been proposed that a metathesis reaction occurs between the dissolved Mn ions and some species in the SEI layer, rather than reduction during Mn deposition on the anode [16]. Even when the deposited Mn compound was not clearly identified, the 2 + oxidation state of Mn deposited on anodes was predominantly observed [9,13,19]. However, recent studies also suggested that a metallic form of Mn can be formed on the anode [14,20,21]. The Mn compounds reported to date are summarized in Table 1.

Despite the research described above, the precise mechanism of the interaction between dissolved Mn ions and the anode/electrolyte interface is still being debated and remains a challenging topic. To shed further light on the mechanism of capacity fade driven by deposited Mn, it is necessary to understand how the dissolved Mn ions cause SEI degradation. The identification and spatial distribution of Mn compounds at the anode/electrolyte interface are also essential to understand the mechanisms of Mn deposition as well as the Mn-induced SEI degradation. The goals of

Table 1
Summary of Mn compounds proposed to be deposited on the anode.

Detection techniques	Electrolyte employed	Proposed Mn compounds	Reference
XPS	1M $LiClO_4$ in EC/DEC with addition of 150 ppm $Mn(ClO_4)_2$	MnO or Mn_2O_3	S. Komaba et al. [13]
XPS	1M $LiPF_6$ in EC/DEC	MnO or MnO_2	L. Yang et al. [19]
XPS AFM	1M $LiClO_4$ in EC/DEC with 100 ppm Mn ions by the anodic dissolution of Mn metal (electrolysis)	Metallic Mn, $MnCO_3$, and $Mn(ClO_4)_2$	M. Ochida et al. [14]
XAS	1M $LiClO_4$ in EC/DEC with addition of 2.5 mM $Mn(ClO_4)_2$	Mn(II) such as $MnCO_3$	C. Delacourt et al. [9]
XAS XPS	1.2M $LiPF_6$ in EC/EMC with 20 ppm Mn ions dissolved from $LiMn_2O_4$ powder	Mn(II) such as $MnCO_3$ and MnF_2	C. Zhan et al. [16]
TEM XPS	1M $LiPF_6$ in EC/DEC	Metallic Mn and MnF_2	X. Xiao et al. [21]
XAS	1M $LiClO_4$ in EC/DEC with addition of 200 ppm $Mn(ClO_4)_2$	Metallic Mn and Mn(II)	S. R. Gowda et al. [20]

this work are an understanding of how the composition and structure of the SEI layer are modified by dissolved Mn ions and how these modifications degrade battery performance. In order to reveal the deposition/reaction mechanism of dissolved Mn ions, we identified the Mn compounds that form on both the graphite anode and individual SEI species, and investigated how the Mn is distributed at the graphite/electrolyte interface.

2. Experimental

A binder-free highly oriented pyrolytic graphite (HOPG, SPI supplies) was chosen as the working electrode in order to investigate the difference in SEI layer compositions that forms in the Mn-free electrolyte and the Mn-containing electrolyte. The presence of polyvinylidenedifluoride (PVdF) in conventional composite anodes makes it difficult to achieve a detailed and conclusive analysis of the SEI composition, since peaks associated with the PVdF binder overlap with the peaks of SEI chemical species in X-ray photoelectron spectroscopy (XPS) spectra. The HOPG electrode was prepared as a square sheet with sides of 5 mm and a thickness of 1 mm. For other purposes, the composite electrode was prepared by spreading a mixture of 90 wt % synthetic graphite powder (TIMREX SLP 30, Timcal) and 10 wt % PVdF binder dissolved in anhydrous N-methyl-2-pyrrolidone (99.5% NMP, Sigma–Aldrich) onto a 9 μm-thick Cu foil (MTI corp.). The electrode sheet was then vacuum-dried at 110 °C for one day to remove the NMP. Lithium metal (Alfa Aesar) and the Celgard 2320 were used as a counter electrode and a separator, respectively, in the coin-cell assembly process. All 2032-type coin cells (MTI Corp.) were assembled in an argon-filled glove box (MBraun) containing less than 0.1 ppm oxygen and moisture. The electrolyte solution was 1 M lithium hexafluorophosphate ($LiPF_6$, Sigma–Aldrich) dissolved in a mixture (1:1, v/v) of ethylene carbonate (EC, Sigma–Aldrich) and dimethyl carbonate (DMC, Sigma–Aldrich). The Mn-containing electrolyte was prepared by dissolving a known amount of synthesized manganese hexafluorophosphate [$Mn(PF_6)_2$] into the base electrolyte. The $Mn(PF_6)_2$ salt was synthesized by reacting manganese chloride ($MnCl_2$, Sigma–Aldrich) with the silver hexafluorophosphate ($AgPF_6$, Sigma–Aldrich) in ethanol. The mixture was then filtered and distilled to isolate the synthesized $Mn(PF_6)_2$. The $Mn(PF_6)_2$ was vacuum-dried at 90 °C overnight before use. The concentration of dissolved Mn ions in the electrolyte was analyzed using inductively coupled plasma optical emission spectrometry (ICP-OES).

For the investigation of cycling performance and SEI composition, the assembled HOPG/Li cells containing the Mn-free or the Mn-containing (200 ppm) electrolyte were charged to 0.01 V and then galvanostatically discharged to 1.5 V at a rate of C/15 in the first 3 cycles, followed by 25 times between 0.01 and 1 V at a rate of C/7, using a battery test system (Biologic). The open-circuited cells at 1.0 V were disassembled in an argon-filled glove box.

For the identification of the deposited Mn compound, the composite electrode cell was charged at a rate of C/15 to 1.0 V, which is below the standard redox potential of Mn/Mn^{2+} (1.87 V vs. Li/Li^+), and then held there for 24 h. This condition was used to examine whether or not the Mn ions were reduced and deposited as metallic Mn under the reduction conditions. To prevent other effects caused by solvent reduction, the potential was held at 1.0 V, which is higher than the known solvent reduction potential 0.8 V. In addition, the cell held at 1.0 V was discharged at a rate of C/15 to 2.5 V, which is above the redox potential, and then kept at this potential for 24 h. Under this condition, oxidation is expected to be favorable at the anode surface. To clearly identify the chemical state of the deposited Mn, we used an electrolyte with a dissolved Mn ion concentration of around 2500 ppm.

To investigate the ion-exchange mechanism, lithium fluoride (LiF, Sigma–Aldrich), which is known to be one of the main components of the SEI, was immersed in both the Mn-free electrolyte and the Mn-containing electrolyte for one week. After soaking, the LiF was extracted from the electrolytes, and then vacuum dried overnight. The same procedure was performed using lithium carbonate (Li_2CO_3, Sigma–Aldrich), except for the storage time. Due to the lower solubility of Li_2CO_3 in the electrolyte, compared with LiF, the Li_2CO_3 was immersed for two weeks [22]. To exclude the possibility of HF reacting with the dissolved Mn ions, lithium perchlorate ($LiClO_4$, Sigma–Aldrich) was used as a salt and manganese perchlorate ($Mn(ClO_4)_2$, Sigma–Aldrich) was added to the electrolyte (1M $LiClO_4$ in EC:DMC (1:1, v/v)). The received $Mn(ClO_4)_2 \cdot 6H_2O$ was vacuum-dried at 100 °C for 24 h to remove any hydrated water residue.

For the investigation of the Mn distribution throughout the SEI layer, a composite electrode with Mn-containing electrolyte (2500 ppm) was cycled five times at a rate of C/15 and charged to 0.005 V. Then, it was stored at open-circuit potential for 1 month at room temperature.

Except for the samples taken to identify the Mn compounds that form on the anode and salts (LiF and Li_2CO_3), other cycled samples (HOPGs) were rinsed with the DMC solvent for 3 min to remove residual salts on samples. Rinsed and non-rinsed samples were vacuum-dried overnight and vacuum-sealed in a glove box in order to transfer them to the XPS instrument for the chemical analysis of the layer that formed during the experiment. XPS measurements were conducted using a Kratos Axis Ultra X-ray photoelectron spectrometer equipped with a monochromatic Al Kα excitation source ($h\nu$ = 1486.6 eV) in the University of Michigan Electron Microbeam Analysis Laboratory (EMAL). The area of the SEI layer analyzed was 300 × 700 μm^2. The binding energy scale was

calibrated from intrinsic hydrocarbon contamination using the C 1s peak at 285 eV. Core spectra were recorded with 20 eV and 40 eV constant pass energy. The fitting of core peaks were performed using the Shirley background correction and Gaussian–Lorentzian curve synthesis (70% Gaussian, 30% Lorentzian). Charge neutralization was used during the measurements. Depth profiles were obtained by Ar-ion beam sputtering using an ion beam voltage of 4 keV.

Atomic force microscopy (AFM) was carried out on the HOPG sample to get the thickness profile of the SEI layer. After the 10th cycle, a square area of 2 × 2 μm^2 was scratched out in the contact mode at a constant force of 500 nN in order to remove the SEI layer from the surface. In the lateral force mode, the area was scraped off until the non-uniform friction, which was due to the SEI, changed to uniform friction, allowing observation of the appearance of the flat HOPG surface. Then, an area of 6 × 6 μm^2 which contains the scratched area was scanned again with a force less than 500 nN. Finally, 20 scan lines in the dotted square area of the height image were averaged to get the average height profile (Fig. 6), since the non-uniform SEI layer made it difficult to determine the SEI layer thickness.

3. Results and discussion

3.1. Influence of dissolved Mn ions on the degradation of the HOPG/Li cell capacity

Fig. 2 shows the cycling performance of HOPG/Li cells containing electrolytes with or without dissolved Mn ions, after the formation cycle. With the addition of dissolved Mn ions at a concentration of 200 ppm, the capacity degradation occurs more severely over 25 cycles. After 25th cycle, the Mn-free cells retain 85% of their original capacity, while the Mn-containing cells retain only 70%. The decrease in reversible capacity due the addition of Mn ions is consistent with the findings of other studies [12,13,16]. According to the previous studies, side reactions related to the deposition of Mn that accompanies the loss of electric charge are the main contributors to the reduction in capacity [23]. In addition, continuous decomposition products of the electrolyte induced by the deposited Mn compounds may hinder the intercalation of lithium into the graphite, thereby reducing the reversibility of the lithium intercalation [12]. It has also been suggested that the capacity fade is caused by modification of the SEI layer, which is continuously reacting with dissolved Mn ions [16]. The capacity

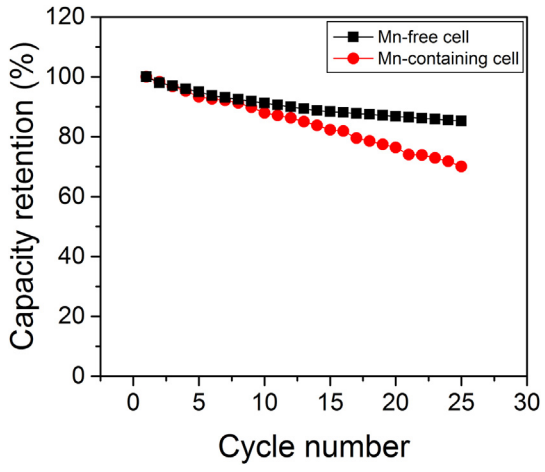

Fig. 2. Discharge capacity retention of the HOPG/Li cell without/with dissolved Mn ions (200 ppm).

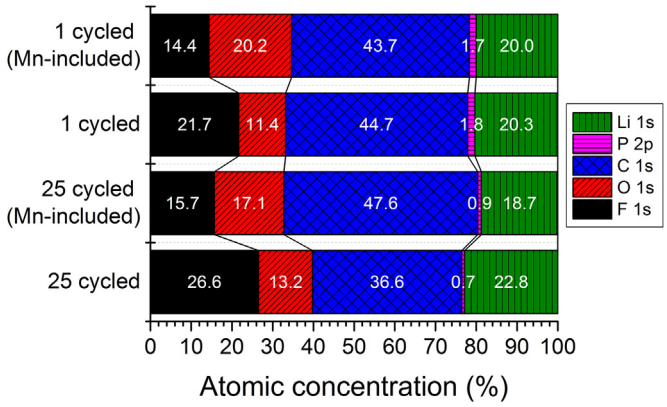

Fig. 3. Comparison of the elemental compositions (atom %) of SEI layers formed in Mn-free and the Mn-containing electrolytes after the 1st cycle and the 25th cycle.

degradation of the cell due to the addition of Mn ions could be even more severe in a full-cell, such as a graphite/$LiMn_2O_4$ cell, which has an absolute capacity. The reduction in the number of cyclable lithium ions caused by the deposition of Mn and SEI reformation/growth additionally contributes to the capacity fade. In the graphite/Li half-cell used in this study, the capacity loss caused by the consumption of cyclable lithium is not considered due to the abundance of cyclable lithium.

3.2. Effects of the dissolved Mn ions on SEI chemical composition and growth

The differences between the SEI layers that form in electrolytes with and without Mn ions can be assessed by investigating the elemental compositions of these SEI layers. Fig. 3 shows the relative amounts of the elements present in the SEI layers that form in Mn-free and the Mn-containing electrolytes after the 1st and 25th cycles. Note that the concentration of Mn cannot be determined in the Mn-containing (200 ppm) cells, since the Mn signal is barely detectable. It seems that the quantity of deposited Mn is below the detection limit (~1000 ppm) of XPS [11]. In reality, the Mn signal can be detected after a very long data-collection time (above 100 core scans), indicating that a very small concentration of Mn (below 0.1%) exists at the surface. Nevertheless, there is a noticeable difference in the chemical compositions of the SEI layers that form in the presence of electrolytes with and without dissolved Mn ions. The SEI layer that forms in the Mn-containing electrolyte contains a higher concentration of oxygen, but a lower concentration of fluorine, than the SEI layer that forms in the presence of the Mn-free electrolyte. The difference in SEI composition is due to the formation of a number of oxygen-containing products caused by the Mn deposition. The oxygen-rich SEI layer might be attributed to either the deposition of oxygen-containing manganese compounds, such as MnO, Mn_2O_3, or $MnCO_3$, or the deposition of additional solvent decomposition products that result from the catalytic effect of the deposited Mn compounds. It has been reported that manganese compounds act as oxidation catalysts, promoting organic compound decomposition [12,24]. Since a very low Mn concentration (below 0.1%) is found in the SEI layer that forms in the Mn-containing electrolyte, the increased amount of oxygen in the Mn-containing cell must be mainly due to the formation of more oxygen-containing organic/polymeric compounds, not oxygen-containing Mn compounds. In the Mn-containing cell, the relative amounts of carbon and oxygen in the SEI layer are still significant after 25 cycles. On the other hand, a lower amount of carbon and a similar amount of oxygen are observed in the SEI layer

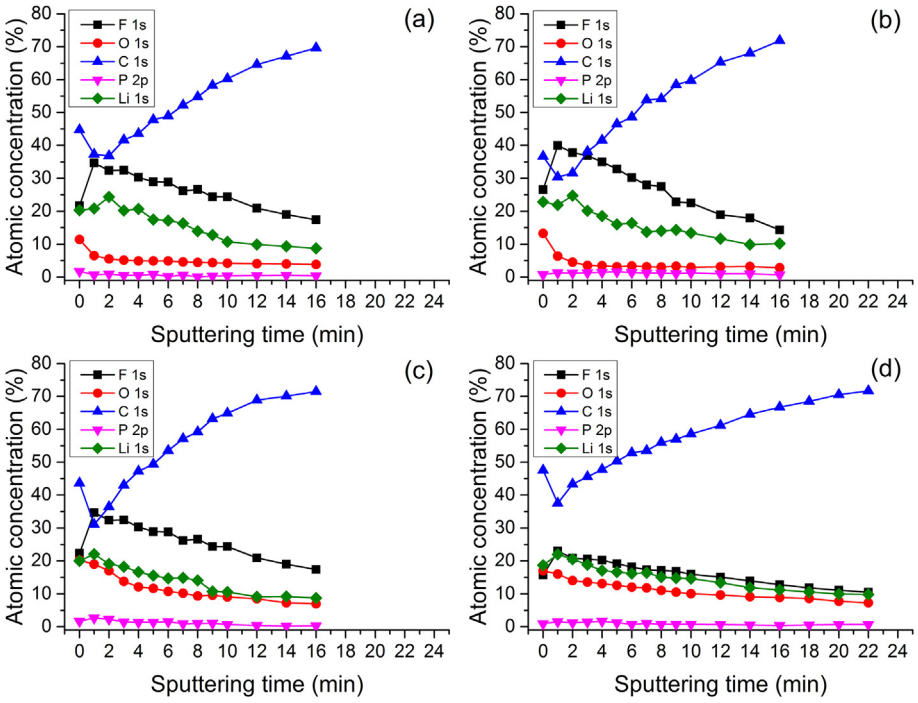

Fig. 4. Depth profiles of HOPG surfaces after: (a) the 1st cycle, (b) the 25th cycle in Mn-free electrolyte; as well as after: (c) the 1st cycle, and (d) the 25th cycle in Mn-containing electrolyte.

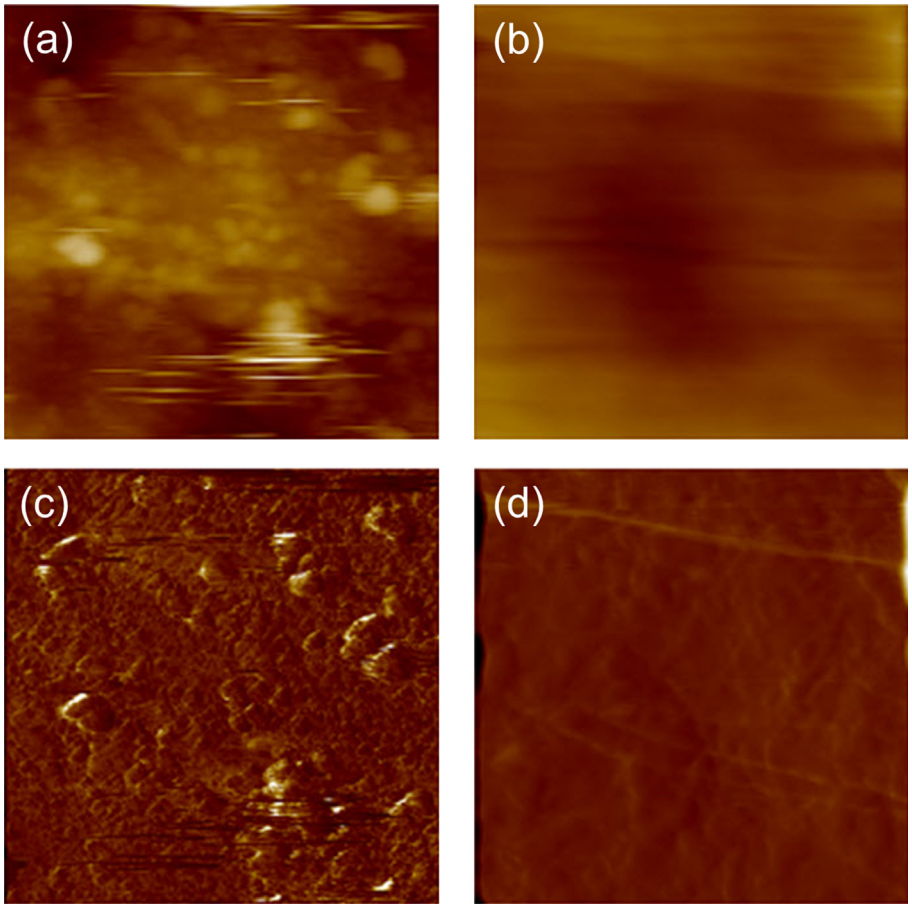

Fig. 5. AFM height (a, b) and friction (c, d) images ($2 \times 2\ \mu m^2$) of HOPG after 10 cycles in Mn-free electrolyte before scratching (a, c) and after scratching (b, d).

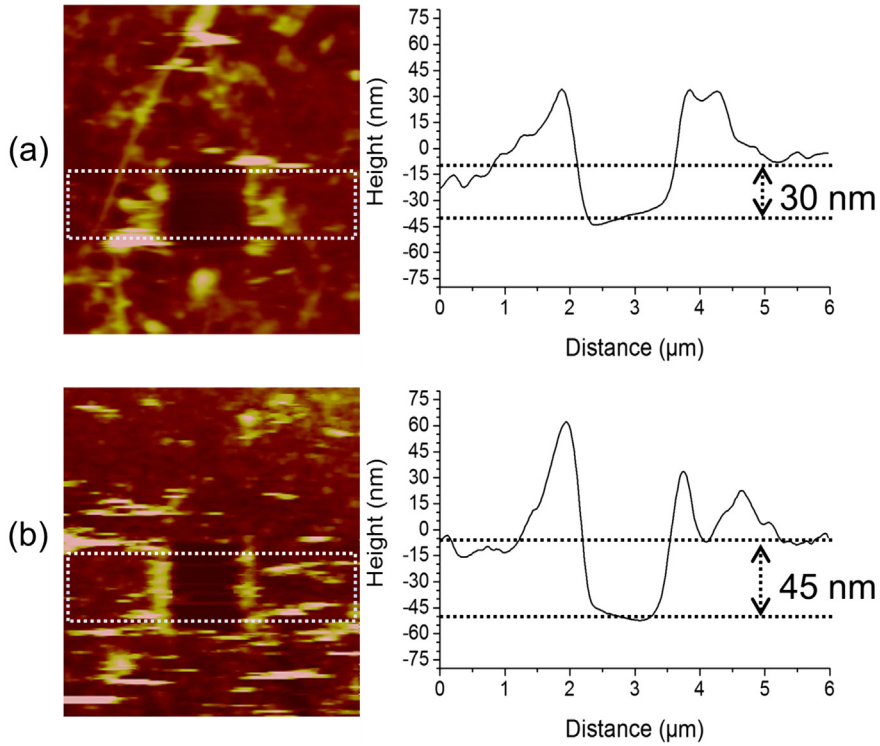

Fig. 6. AFM height images and their corresponding averaged cross–sectional profiles of HOPGs cycled in (a) Mn-free electrolyte and (b) Mn-containing electrolyte.

that forms in the presence of Mn-free electrolyte after 25 cycles. It seems that the content of LiF increases considerably in the SEI layer during cycling, resulting in a significant increase in the quantity of fluorine in the Mn-free electrolyte. In contrast, a small increase in the fluoride content of the SEI layer that forms in Mn-containing electrolyte after 25 cycles indicates that the amount of organic/polymeric components (which consist of carbon and oxygen) in the SEI layer is greater than the increased amount of LiF over cycling. This also suggests that the SEI layer that forms in the Mn-containing electrolyte includes more organic/polymeric compounds (containing C and O) than the SEI layer that forms in the Mn-free electrolyte. This finding is further supported by the results of depth profiling (Fig. 4). In the Mn-free cell, the amount of oxygen rapidly decreases after only 2 min of sputtering, declining below half the initial amount of oxygen. The observed trend of decreasing oxygen is consistent with the results of other studies [25–28]. In the Mn-containing cell, however, the oxygen content decreases more gradually, requiring 8–10 min of sputtering in order to decline below half the initial oxygen concentration. It is known that the initial decrease in oxygen content mainly originates from the removal of polymer and solvent reduction products, such as polyethylene oxide (PEO) and alkyl carbonates [25–27]. Thus, this result indicates that more oxygen-containing products (possibly the organic/polymeric compounds) are present in the deeper SEI layer that forms in the Mn-containing cell. As mentioned above, since the quantity of Mn compounds observed in the SEI layer is extremely low, the contribution of oxygen-containing Mn compounds to the change in the oxygen content is negligible. Except for the oxygen, the changes in other elements as a function of depth are very similar in the Mn-free and the Mn-containing cells, following the generally observed trends [25–28]. The concentration of carbon initially decreases, which reflects the reduction of organic/polymeric species, and then increases with sputtering time, due to the contribution of the gradual exposure of the HOPG underlying the SEI layer. The initial increases in fluorine and lithium reflect the increase in LiF content with the decrease in the organic/polymeric thin layer. The fluorine content decreases continuously with the gradual removal of LiF, while the lithium content decreases due to the reduction of lithium-containing organic and inorganic components, such as alkyl carbonates and Li_2CO_3.

Based on the sputtering time needed for the carbon content to exceed 70%, the thickness of the SEI layer that forms in the Mn-containing electrolyte can be compared to that of the SEI layer that forms in the Mn-free electrolyte. After the 1st cycle, the thickness of the SEI layer that forms in the presence of Mn-containing electrolyte (Fig. 4c) is quite similar to that of the SEI layer that forms in the presence of the Mn-free electrolyte (Fig. 4a). It is well known that SEI formation mostly occurs in the 1st cycle, due to the reduction of the electrolyte. Thus, this result indicates that the influence of the dissolved Mn ions on the initial SEI layer growth is not significant during the formation process. However, the effect is clearly seen after the 25th cycle. In the Mn-free cell, the thickness of the SEI layer after the 25th cycle (Fig. 4b) is almost identical with the thickness of the SEI layer after the 1st cycle (Fig. 4a). This result suggests that the SEI layer that forms without deposited Mn effectively suppresses further electrolyte decomposition, thereby limiting SEI growth. In contrast to the normal SEI layer, the SEI layer that forms with deposited Mn allows additional electrolyte decomposition over repeated cycles, showing a thicker SEI layer after the 25th cycle (Fig. 4d) than after the 1st cycle (Fig 4c). The instability of the SEI layer due to the deposited Mn leads to the continuous growth of the SEI layer during cycling. As mentioned earlier, it is quite likely that the Mn compounds deposited in the SEI layer act as oxidation catalysts, promoting further electrolyte decomposition. As shown in the depth profile of the SEI layer that forms in the presence of Mn-containing electrolyte after the 25th cycle, a considerable amount of oxygen-containing products are deeply distributed throughout the outer

part of SEI layer. This supports the possibility that deposited Mn compounds catalyze the decomposition of organic compounds.

The increase in SEI thickness due to Mn deposition is also confirmed by AFM measurements. Fig. 5 shows the changes in the AFM height and friction images on a HOPG cycled in Mn-free electrolyte. Non-uniform particle-like precipitates (SEI layer) form on the flat HOPG surface after cycling, which is consistent with the results of other studies [2,14,15]. In the lateral (friction) signals, the non-uniform friction image after cycling also indicates that the SEI layer completely covers the HOPG surface. After scraping the layer off using several repeated scans, the height and friction images of the scraped area become almost uniform, indicating that the HOPG surface is fully exposed. The thickness of the SEI layer is estimated from the difference in height between the scratched and unscratched areas (Fig. 6). Due to the roughness of the SEI layer, the 20 scan lines in the dotted square area of the height image were averaged to get the average SEI height profile. It seems that the hills observed near the left and right of the scraped area are formed by the accumulation of material from the SEI layer removed during the scratching process. The thickness of the SEI layer formed in the presence of Mn-containing electrolyte is estimated to be roughly 45 nm, while the SEI layer formed in the presence of the Mn-free electrolyte has a thickness of about 30 nm. This implies that deposited Mn promotes electrolyte decomposition, resulting in a thicker SEI layer, which is consistent with the result obtained using XPS depth profiles.

In order to further investigate the changes in SEI composition resulting from the deposited Mn compounds, high-resolution XPS spectra after the 25th cycle are compared (Fig. 7). In the C 1s spectra, the peak at 284.3 eV, assigned to graphite, is not observed, indicating that the HOPG surface is fully covered by the SEI layer. The C 1s spectra can be deconvoluted into three main peaks with an additional shoulder. The first peak, at 285.0 eV, is attributed to intrinsic hydrocarbons and alkane products (C—C and C—H bonds) [29,30]. The second peak, at 286.3 eV with a small shoulder at 287.3 eV, could be assigned to ether carbons within the oligomeric polyethylene oxide (PEO) species $(-CH_2-CH_2-O-)_n$ and the lithium alkyl carbonates ($ROCO_2Li$). The presence of PEO and $ROCO_2Li$ in the SEI layer has been widely described in the literature [27–32]. The third peak, at 289.5 eV, which corresponds to $-CO_3-$ bonds, is associated with carbonate species such as lithium carbonate (Li_2CO_3) and lithium alkyl carbonate ($ROCO_2Li$) [27–32]. In the Mn-containing cell, this peak may also be associated with manganese carbonate ($MnCO_3$), which may have been deposited on the anode. Unfortunately, it is difficult to verify the presence of $MnCO_3$, since the peak at 289.5 V is relatively weak and broad. Based on the analysis of the C 1s spectra, the SEI species that form in the Mn-containing electrolyte are similar to those that form in the Mn-free electrolyte. However, the relatively high intensity is seen in the 286–287 eV region of the XPS spectrum of the sample cycled in the presence of the Mn-containing electrolyte, compared with the sample cycled in the Mn-free electrolyte. This result indicates that a considerable amount of organic species, such as PEO and $ROCO_2Li$, are formed during cycling in the Mn-containing cell. The increase of these compounds explains the formation of the oxygen-rich SEI layer in the Mn-containing cell, which is shown in Figs. 3 and 4. Thus, these results provide additional evidence that the deposition of Mn compounds induces a greater amount of organic compound decomposition.

Noticeable differences are also observed in the F 1s and the P 2p spectra of the Mn-free and the Mn-containing samples. The F 1s spectra show that the SEI layers of both samples are composed of salt decomposition products, such as Li_xPF_y and/or $Li_xPF_yO_z$ (687.4 eV), and LiF (685.4 eV) [29]. The dominant peak from the sample cycled in the presence of the Mn-containing electrolyte is broadened and shifted to a higher binding energy (685.9 eV). This is also observed in the sample cycled in the presence of the Mn-free electrolyte. The broadened and shifted peak might be attributed to the presence of an additional compound near the peak at 685.9 eV. We suspect that the formation of MnF_2 might contribute to this shifting and broadening of the dominant peak. The P 2p spectra of both samples show two distinct peaks at 137.3 eV and 134.2 eV, regardless of the presence of deposited Mn. The peak at 137.3 eV can be assigned to an insoluble P—F compound (Li_xPF_y). The peak at 134.2 eV can be associated with $Li_xPF_yO_z$ compounds such as Li_2PFO_3 $LiPOF_2$, and/or phosphate compounds such as

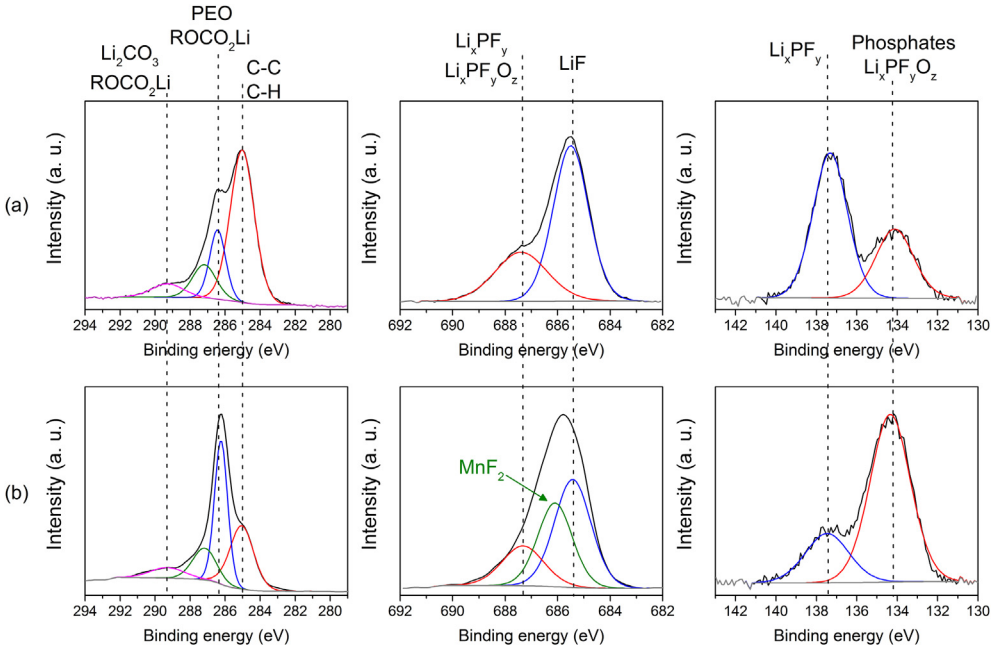

Fig. 7. C 1s, F 1s, and P 2p XPS spectra of HOPGs cycled 25 times with: (a) Mn-free electrolyte and (b) Mn-containing electrolyte.

phosphate-ending PEO oligomer species [29–31]. The sample cycled in the Mn-containing electrolyte shows that the intensity of the peak at 134.2 eV increases relative to that of the peak at 137.3 eV. The increase in peak intensity at 134.2 eV indicates that more decomposition products of $LiPF_6$ are produced in the presence of the deposition of Mn compounds. This observation is similar to the results from samples cycled at high temperatures [29]. It has been reported that $LiPF_6$ decomposition considerably increases at high temperatures. In addition, the reaction between highly reactive PF_5 and solvents produces some polymeric species [29,33]. It seems that the deposition of Mn compounds causes $LiPF_6$ instability, which could be another mechanism by which polymeric species are generated.

3.3. Identification of the Mn compounds that are deposited on the anode

To positively identify the Mn compounds that are deposited on the anode, a high concentration of Mn ions was dissolved in the electrolyte. As shown in Fig. 8, the amount of Mn compounds deposited increases as the concentration of Mn ions in the electrolyte increases. When the electrolyte contains Mn ions at a concentration of 200 ppm, the intensity of the peak corresponding to Mn is extremely low (almost invisible in the survey spectrum). Therefore, a considerably long scan time is required to detect the Mn signal in the core spectrum. The insufficient intensity of the Mn spectra may cause misinterpretation of the chemical state of the manganese species deposited on the anode, since determination of the position of the Mn $2p_{3/2}$ peak is confusing in the Mn 2p spectrum. Due to blurred signals in the XPS spectra caused by the small amount of Mn deposited on the anode, previous studies have experienced difficulties in conclusively identifying the deposited Mn compound [11,13,19]. With a high concentration of dissolved Mn-ions (around 2500 ppm) in the electrolyte, the relative concentration of the element Mn on the anode surface is determined to be 2.2%, showing a clear Mn signal in the survey spectrum. The multiplet splitting of Mn 2p and Mn 3s peaks, in addition to the position of the Mn $2p_{3/2}$ peak are analyzed in an attempt to confirm the chemical state of the deposited Mn.

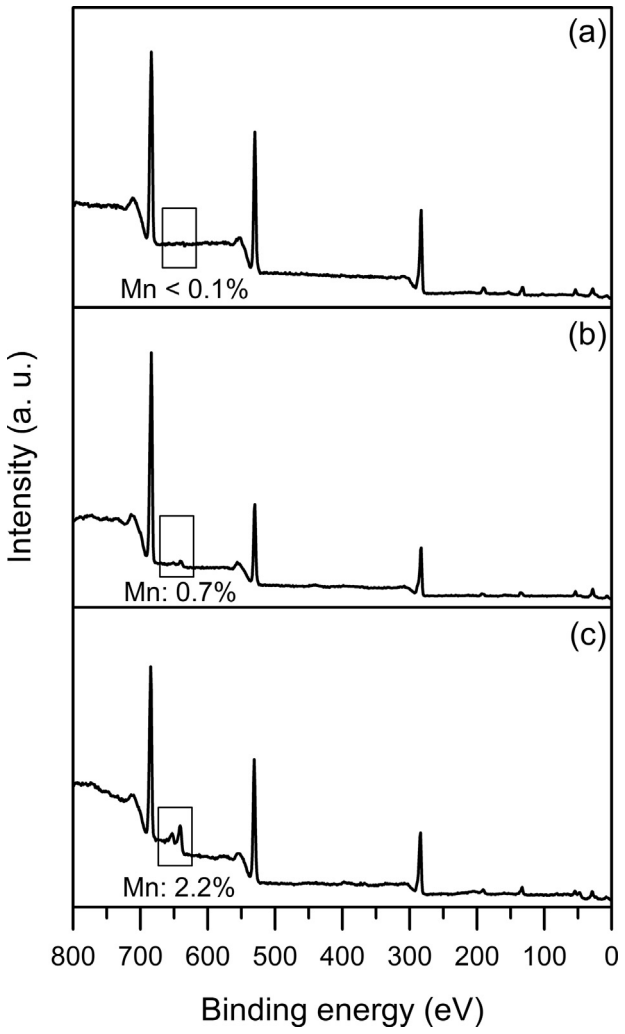

Fig. 8. XPS survey spectra of negative electrodes after the 1st cycle in the presence of electrolytes containing Mn ions at concentrations of: (a) 200 ppm, (b) 1000 ppm, and (c) 2500 ppm.

It is believed that the dissolved Mn-ions may be reduced to form Mn metal during the deposition because of the standard redox potential of the Mn to Mn(||) transition (1.87 V vs. Li/Li^+). To assess the electrochemical reduction of Mn-ions driven by the lowered potential, the cell is charged to 1.0 V, which is below the redox potential 1.87 V, and then kept at this potential for 24 h. To prevent the influence of solvent reductions on the deposition of Mn, the cell is not charged below 1.0 V. It is commonly known that solvent reduction begins near 0.8 V. Under this condition, which favors reduction at the anode surface, MnF_2 is mainly formed; metallic Mn is not deposited on the anode surface (Fig. 9). The asymmetry of the dominant peak (685.3 eV) in the F 1s spectrum (Fig. 9 (a)) may be due to contributions from both LiF and MnF_2 (near 685.8 eV) formed on the surface. The formation of MnF_2 is also supported by analyses of the Mn 2p and Mn 3s spectra. In the Mn 2p core spectrum, the peak maximum of Mn $2p_{3/2}$ is observed at around 642.9 eV, which is very close to the maxima found in our reference MnF_2 (643 eV) and in other reports (642.7, 642.8 eV) [34,35]. This peak position is far from that expected for metallic Mn (639.2 eV) and clearly higher than those observed for other Mn compounds, such as MnO (641.5, 641.7 eV) and $MnCO_3$ (642 eV) [34–36]. In addition, the multiplet splitting of the Mn 2p peak, which is the difference in binding energy between the Mn $2p_{1/2}$ and the Mn $2p_{3/2}$, is 12.2 eV. The observed value is higher than the values found in metallic Mn (11.0 eV) and MnO (11.6 eV) [37,38]. The observed value is similar to the values found for $MnCO_3$ (12.2 eV) and MnF_2 (12.1 eV), which are measured in our reference samples. The presence of MnF_2 on the surface is further confirmed by the observed multiplet splitting of the Mn 3s (6.5 eV) peak, which is the same as the values measured for the reference MnF_2 (6.5 eV) in this study and close to the values found in previous reports (6.3, 6.5 eV) [35,39]. The observed multiplet splitting of the Mn 3s peak is significantly different than the value observed for metallic Mn (3.7 eV) [40]. The measured reference $MnCO_3$ shows a lower value (6.1 eV) and the values reported for other possible Mn compounds, such as MnO (5.5 eV), Mn_2O_3 (5.4 eV), and MnO_2 (4.6 eV), are considerably lower than the observed value (6.5 eV) [35]. Based on these observations, we believe that the majority of Mn is deposited in the form of MnF_2 particles, not metallic Mn. Our observation of MnF_2 formation is consistent with the results of a recent study [21]. They used TEM images to demonstrate that MnF_2 nanoparticles were formed at the graphite/electrolyte interface. However, it is possible that small amounts of the metallic Mn and other Mn compounds, such as $MnCO_3$ and the MnO, exist on the anode surface, as suggested by other researchers [9,14,20]. Note that the formation of Mn metal is mainly detected in the $LiClO_4$-based cells, as summarized in Table 1. This suggests that Mn metal might be formed predominantly in $LiClO_4$-based cells, rather than $LiPF_6$-based cells. In $LiPF_6$-based cells, MnF_2 compounds, which play the

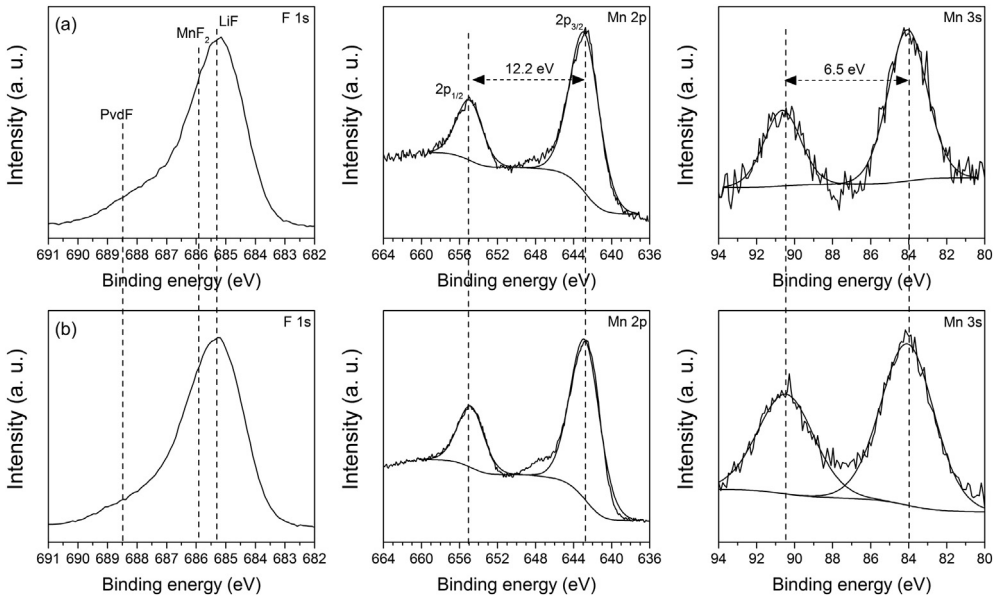

Fig. 9. F 1s, Mn 2p, Mn 3s spectra of composite electrodes held for 24 h at (a) 1.0 V during the 1st charge (i.e., reductive condition at the anode) and (b) 2.5 V during the 1st discharge after the potential is held at 1.0 V (i.e., oxidative condition at the anode).

role of an electric insulator, seem to be formed initially on the surface, suppressing the further formation of metallic Mn on the surface [21].

To construct conditions favorable for oxidation at the anode surface, the cell is charged and held at 1.0 V, and then discharged and kept at 2.5 V, which is higher than the standard redox potential of Mn/Mn(||). As shown in Fig. 9 (b), the MnF_2 that forms is not changed significantly, due to the oxidative conditions at the anode. This result indicates that the formation of MnF_2 on the anode surface is an irreversible reaction. It seems that the deposition of Mn ions and the formation of Mn compounds are not significantly affected by redox reactions or anode potentials, as suggested by a recent study [16]. They proposed that a metathesis reaction occurs between Mn ions and species in the SEI layer at the anode surface during Mn deposition, rather than a reduction reaction. Consistent with the study, we speculate that LiF in the SEI layer can react with the Mn^{2+} ions to form MnF_2 according to the following reactions:

$$LiPF_6 \leftrightarrow LiF(s) + PF_5 \quad (1)$$

$$2LiF + Mn^{2+} \rightarrow MnF_2 + 2Li \quad (2)$$

Alternatively, MnF_2 can be formed due to the acid HF environment. It has been suggested that the acid HF is considered as the main reason for MnF_2 formation on the cathode. The mechanism of MnF_2 formation on the cathode is as follows [41]:

$$2LiMn_2O_4 + 4HF \rightarrow 3MnO_2 + MnF_2 + 2LiF + 2H_2O \quad (3)$$

In a similar manner, the formation of MnF_2 can occur at the anode according to the following series of reactions:

$$LiPF_6 \leftrightarrow LiF(s) + PF_5 \quad (4)$$

$$PF_5 + H_2O \rightarrow POF_3 + 2HF \quad (5)$$

$$2HF + Mn^{2+} \rightarrow MnF_2 + H_2 \quad (6)$$

Thus, we believe that MnF_2 formation is caused by either ion-exchange reactions or the reactions of HF with Mn ions.

3.4. Mechanism of the formation of Mn compounds on the graphite anode

Two potential mechanisms of MnF_2 formation were introduced in the previous section. One involves ion-exchange reactions with Mn ions, and the other involves the reaction of HF with Mn ions. To elucidate the mechanism of the formation of Mn compounds, LiF and Li_2CO_3, which are known to be the main SEI products that form on the anode, were immersed in the Mn-containing electrolyte. To exclude the possibility of the HF-induced reaction mechanism, we used $LiClO_4$ and $Mn(ClO_4)_2$ salts, instead of $LiPF_6$ and $Mn(PF_6)_2$ salts in the electrolyte. Fig. 10 shows that LiF powder (685.3 eV in F 1s spectrum) does not change its binding energy in the presence of a normal electrolyte. The intensity of the LiF in the electrolyte is slightly reduced compared with that of bare LiF, since the residual solvents and decomposition products cover the LiF powder. However, the peak associated with LiF is shifted to higher binding energy (685.8 eV) in the Mn-containing electrolyte. The peak observed at the higher binding energy can be explained by the fact that the fluorine is bonded to manganese, which has a higher electronegativity than lithium. This result indicates that LiF reacts

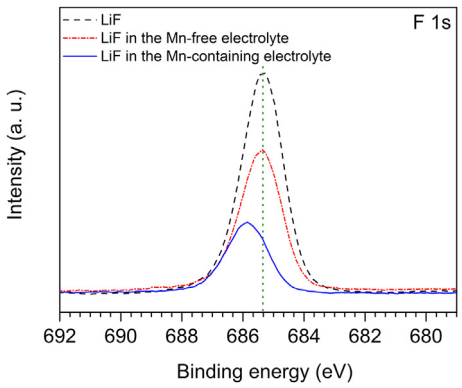

Fig. 10. Changes in the F 1s spectrum of LiF after soaking in an electrolyte with or without Mn ions.

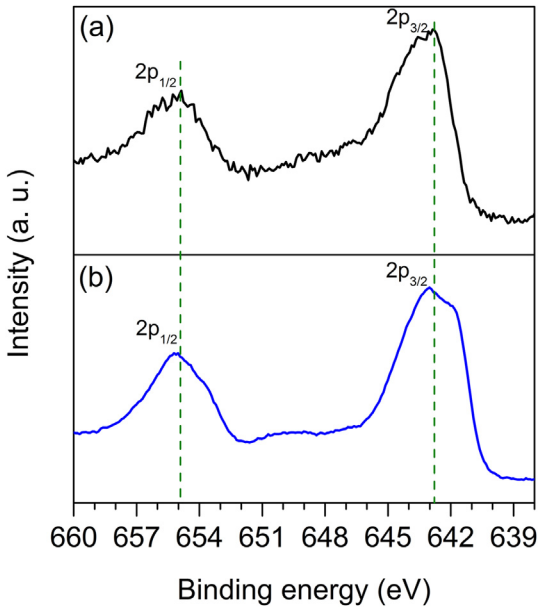

Fig. 11. Comparison of the Mn 2p spectra of (a) LiF soaked in Mn-containing electrolyte and (b) a reference sample of MnF_2.

with Mn ions in the electrolyte, forming MnF_2. The formation of MnF_2 is confirmed by the Mn 2p spectrum shown in Fig. 11. The Mn 2p spectrum of LiF soaked in the Mn-containing electrolyte is very similar to that of the reference MnF_2 compound. It suggests that a portion of the LiF is converted to MnF_2. Note that the peak intensity in the F 1s spectrum (Fig. 10) decreases more in the Mn-containing electrolyte than in the normal electrolyte. This may indicate that the process responsible for the formation of MnF_2 promotes further solvent decomposition. In conclusion, it is clear that the ion-exchange phenomenon happens between the LiF that forms in the SEI layer and dissolved Mn ions at the graphite/electrolyte interface and that further solvent decomposition can occur during the reaction process.

Soaking Li_2CO_3 powders in Mn-free electrolyte and in Mn-containing electrolyte allows further examination of this mechanism. As shown in Fig. 12, the peak associated with the bare Li_2CO_3 is located at 531.6 eV in the O 1s spectrum. The Li_2CO_3 powder soaked in the Mn-free electrolyte has a dominant peak (533.5 eV) with a small shoulder (531.5–532.5 eV). The shoulder can be assigned to Li_2CO_3, while the peak at 533.5 eV corresponds to carbonate esters ($ROCO_2R'$) that originate from solvent residues and decomposition products, such as lithium alkyl carbonate species. The strong peak is shifted to lower binding energy (533 eV) in the presence of Mn ions in the electrolyte. This may result from an additional contribution from $MnCO_3$ (532.2 eV), which has a slightly higher binding energy than Li_2CO_3 (531.6 eV) [42]. As in the case of LiF, the reduced intensity of the dominant peak is also observed. The Mn 2p spectrum supports the formation of $MnCO_3$. The Mn 2p spectrum collected from the Li_2CO_3 powder soaked in the Mn-containing electroltye resembles that of reference $MnCO_3$, as shown in Fig. 13. The Mn $2p_{3/2}$ peak maximum is located at approximately 642 eV, showing multiplet splitting of 12.2 eV. In addition, the presence of two satellite peaks near both the Mn $2p_{3/2}$ and $2p_{1/2}$ (marked as S in Fig. 13) is very similar to the satellite structure of the reference $MnCO_3$. Satellite structure is an important factor that has been used to identify Mn chemical states. The spectrum of MnO has satellite peaks associated with both the Mn $2p_{3/2}$ and Mn $2p_{1/2}$ peaks, while the spectra of Mn_2O_3 and MnO_2 have satellite peaks associated with only their Mn $2p_{1/2}$ peaks [38]. Although MnO has also two satellite peaks associated with its Mn $2p_{3/2}$ and Mn $2p_{1/2}$ peaks, the peak positions of Mn $2p_{3/2}$ (640.6 eV) and O 1s (529.6 eV) are much lower than those of $MnCO_3$ [38]. This clearly indicates that the observed Mn 2p spectrum corresponds to that of $MnCO_3$, not MnO. Thus, the results show that the Li_2CO_3 is partially converted to $MnCO_3$ through the ion-exchange reaction.

Based on these findings, we propose that reactions can occur

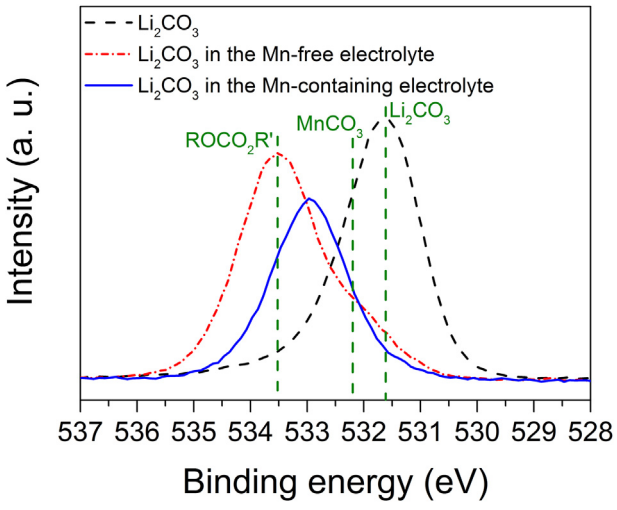

Fig. 12. Changes in the O 1s spectrum of Li_2CO_3 after soaking in an electrolyte with or without Mn ions.

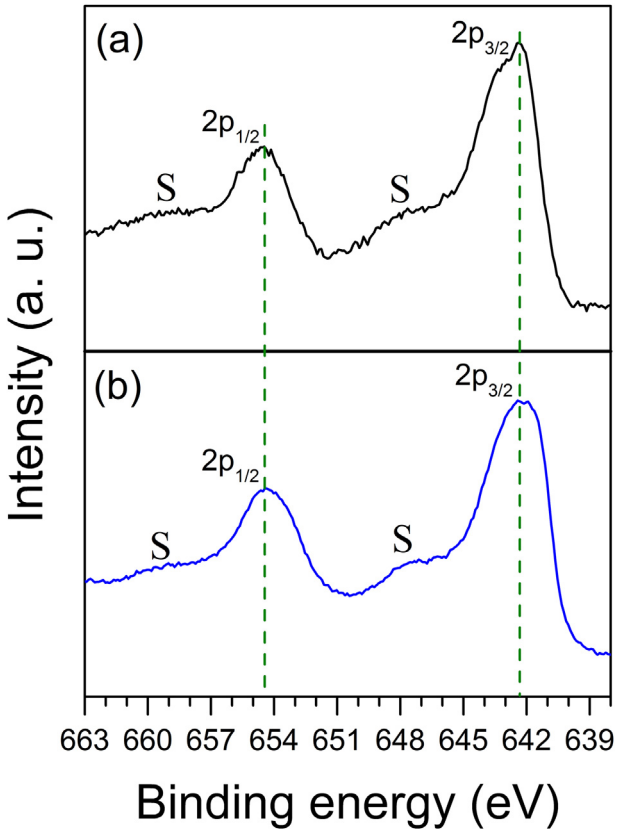

Fig. 13. Comparison of the Mn 2p spectra of (a) Li_2CO_3 soaked in Mn-containing electrolyte and (b) a reference sample of $MnCO_3$.

between inorganic species and dissolved Mn ions, transforming SEI species into diverse Mn compounds, such as MnF_2 and $MnCO_3$. During the reaction process, additional decompositions of the electrolyte may take place at the anode/electrolyte interface.

3.5. Spatial distribution of deposited Mn compounds at the graphite/electrolyte interface

In order to gain further information about the interactions of dissolved Mn ions at the anode/electrolyte interface, it is necessary to understand how the deposited Mn is distributed at the anode/electrolyte interface. Fig. 14 shows the depth profile of the aged anode, revealing the distribution of Mn element throughout the graphite/electrolyte interface. The Mn profile shows that Mn is not uniformly distributed at the graphite/electrolyte interface. A small amount of the Mn is observed at the top surface of the interface, indicating that the deposition of dissolved Mn ions is not severe in the region of the porous organic layer. Mn reaches its maximum after about 60 min of Ar-ion sputtering, at which point the graphite anode starts to appear, as evidenced by a sharp increase in carbon. This result suggests that the dissolved Mn ions are mostly deposited near the inorganic layer/graphite interface, suggesting that the inorganic layer can be significantly affected by the dissolved Mn ions. It seems that the dissolved Mn ions easily diffuse through the porous organic SEI layer and interact with the inorganic species, possibly as a result of the ion-exchange mechanism, as evidenced by previous results. The tendency of Mn accumulation at the inorganic layer/graphite interfacial regions is consistent with the results observed in aged commercial cells [11]. The diffusion of lithium ions may be more hindered by the deposition of inorganic Mn compounds, such as MnF_2 and $MnCO_3$, which can limit the capacity of the Li-ion battery. Note that Mn is still observable at the end of sputtering, at which point the graphite surface is almost fully exposed by removal of the SEI layer. The small amount of Mn that can be detected inside the graphite suggests that dissolved Mn ions may co-intercalate or move into the graphite interlayer via either defects in the SEI layer or cracks in the graphite. It has been recently observed that Mn nanoparticles are present within cracks in the graphite, suggesting that Mn compounds can be deposited internally [21]. In addition, surface structural disordering in the graphite due to deposition of iron has been observed [43]. Although the observed Mn content may be associated with an artifact of the sputtering process that can cause the re-deposition of sputtered Mn, there is a strong possibility that Mn ions are deposited at the interlayer spaces between graphene layers or cracks in graphite, which may inhibit the contraction and expansion of the graphite during the intercalation/deintercalation process. The structural disorder of the graphite due to Mn deposition and its effects are currently under investigation.

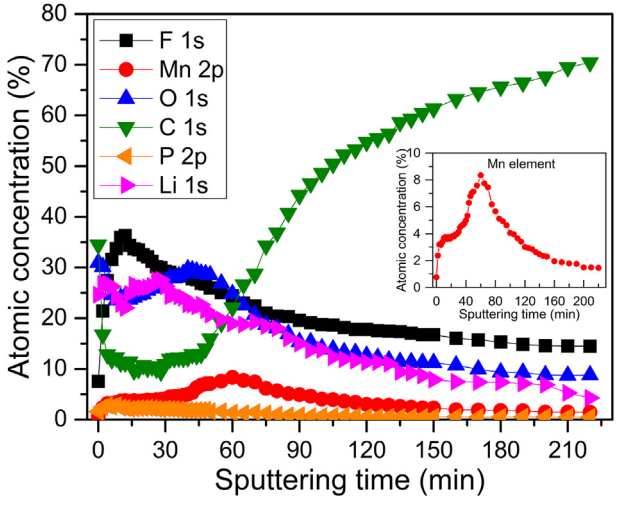

Fig. 14. XPS depth profile of a composite electrode stored for one month after 5 cycles in Mn-containing electrolyte. The inset contains an enlargement of the profile of the Mn element.

4. Conclusions

Deterioration of the SEI layer due to the deposition of dissolved Mn ions significantly contributes to the degradation of Li-ion battery capacity. In this work, the chemical degradation of the SEI layer induced by dissolved Mn ions and its mechanism has been systematically investigated using XPS and AFM. The chemical composition of the SEI layer formed in the presence of dissolved Mn ions shows a more oxygen-rich layer. This layer originates from an increased amount of organic/polymeric species that result from additional electrolyte decompositions catalyzed by Mn deposition and interaction processes of the dissolved Mn ions. XPS and AFM measurements revealed that SEI growth is accelerated by the deposition of dissolved Mn ions, showing a thicker SEI layer on the graphite anode. The dissolved Mn ions easily diffuse through the porous SEI layer and mostly deposit at the inorganic layer/graphite interface, where the Mn ions interact with inorganic SEI species via the ion-exchange mechanism. The main Mn compound formed on the anode surface is identified as MnF_2, which is not much affected by reductive/oxidative conditions. The dissolved Mn ions may diffuse or co-intercalate into graphite through both defects in the SEI layer and cracks in the graphite, which might cause the surface structural disordering in graphite.

The findings from this work deepen our understanding of SEI degradation mechanisms at elevated temperatures. Both the high temperature itself and the increased deposition of dissolved Mn-ions, which is driven by elevated temperatures, significantly affect the instability of the SEI layer. Improving the stability of the SEI layer at elevated temperatures will require strategies that suppress the interaction of dissolved Mn ions with the SEI layer, as well as the development of a thermally stable SEI layer.

Acknowledgments

This research was funded by the GM/UM Advanced Battery Coalition for Drivetrains. Support from our sponsor is gratefully acknowledged. The authors also thank Xiaoguang Hao, a graduate student at the University of Michigan for help with the synthesis of $Mn(PF_6)_2$ salt.

References

[1] J. Vetter, P. Novak, M.R. Wagner, C. Veit, K.C. Moller, J.O. Besenhard, M. Winter, M. Wohlfahrt-Mehrens, C. Vogler, A. Hammouche, J. Power Sources 147 (2005) 269–281.
[2] M. Inaba, H. Tomiyasu, A. Tasaka, S.K. Jeong, Z. Ogumi, Langmuir 20 (2004) 1348–1355.
[3] T. Zheng, A.S. Gozdz, G.G. Amatucci, J. Electrochem. Soc. 146 (1999) 4014–4018.
[4] T. Aoshima, K. Okahara, C. Kiyohara, K. Shizuka, J. Power Sources 97–8 (2001) 377–380.
[5] Y. Terada, Y. Nishiwaki, I. Nakai, F. Nishikawa, J. Power Sources 97–8 (2001) 420–422.
[6] Y. Matsuo, R. Kostecki, F. McLarnon, J. Electrochem. Soc. 148 (2001) A687–A692.
[7] D. Kim, S. Park, O.B. Chae, J.H. Ryu, Y.U. Kim, R.Z. Yin, S.M. Oh, J. Electrochem. Soc. 159 (2012) A193–A197.
[8] I.H. Cho, S.S. Kim, S.C. Shin, N.-S. Choi, Electrochem. Solid St. 13 (2010) A168–A172.
[9] C. Delacourt, A. Kwong, X. Liu, R. Qiao, W.L. Yang, P. Lu, S.J. Harris, V. Srinivasan, J. Electrochem. Soc. 160 (2013) A1099–A1107.

[10] W. Choi, A. Manthiram, J. Electrochem. Soc. 153 (2006) A1760–A1764.
[11] D.P. Abraham, T. Spila, M.M. Furczon, E. Sammann, Electrochem. Solid St. 11 (2008) A226–A228.
[12] S. Komaba, N. Kumagai, Y. Kataoka, Electrochim. Acta 47 (2002) 1229–1239.
[13] S. Komaba, T. Itabashi, T. Ohtsuka, H. Groult, N. Kumagai, B. Kaplan, H. Yashiro, J. Electrochem. Soc. 152 (2005) A937–A946.
[14] M. Ochida, Y. Domi, T. Doi, S. Tsubouchi, H. Nakagawa, T. Yamanaka, T. Abe, Z. Ogumi, J. Electrochem. Soc. 159 (2012) A961–A966.
[15] M. Ochida, T. Doi, Y. Domi, S. Tsubouchi, H. Nakagawa, T. Yamanaka, T. Abe, Z. Ogumi, J. Electrochem. Soc. 160 (2013) A410–A413.
[16] C. Zhan, J. Lu, A. Jeremy Kropf, T. Wu, A.N. Jansen, Y.K. Sun, X. Qiu, K. Amine, Nat. Comms. 4 (2013).
[17] A.V. Plakhotnyk, L. Ernst, R. Schmutzler, J. Fluor. Chem. 126 (2005) 27–31.
[18] K. Amine, J. Liu, S. Kang, I. Belharouak, Y. Hyung, D. Vissers, G. Henriksen, J. Power Sources 129 (2004) 14–19.
[19] L. Yang, M. Takahashi, B.F. Wang, Electrochim. Acta 51 (2006) 3228–3234.
[20] S.R. Gowda, K.G. Gallagher, J.R. Croy, M. Bettge, M.M. Thackeray, M. Balasubramanian, Phys. Chem. Chem. Phys. 16 (2014) 6898–6902.
[21] X. Xiao, Z. Liu, L. Baggetto, G.M. Veith, K.L. More, R.R. Unocic, Phys. Chem. Chem. Phys. 16 (2014) 10398–10402.
[22] K. Tasaki, A. Goldberg, J.J. Lian, M. Walker, A. Timmons, S.J. Harris, J. Electrochem. Soc. 156 (2009) A1019–A1027.
[23] T. Tsujikawa, K. Yabuta, T. Matsushita, M. Arakawa, K. Hayashi, J. Electrochem. Soc. 158 (2011) A322–A325.
[24] Y.F. Shen, R.P. Zerger, R.N. Deguzman, S.L. Suib, L. McCurdy, D.I. Potter, C.L. Oyoung, Science 260 (1993) 511–515.
[25] D. Bar-Tow, E. Peled, L. Burstein, J. Electrochem. Soc. 146 (1999) 824–832.
[26] A.M. Andersson, K. Edstrom, J. Electrochem. Soc. 148 (2001) A1100–A1109.
[27] V. Eshkenazi, E. Peled, L. Burstein, D. Golodnitsky, Solid State Ionics 170 (2004) 83–91.
[28] A.M. Andersson, A. Henningson, H. Siegbahn, U. Jansson, K. Edstrom, J. Power Sources 119 (2003) 522–527.
[29] A.M. Andersson, D.P. Abraham, R. Haasch, S. MacLaren, J. Liu, K. Amine, J. Electrochem. Soc. 149 (2002) A1358–A1369.
[30] R. Dedryvere, S. Laruelle, S. Grugeon, L. Gireaud, J.M. Tarascon, D. Gonbeau, J. Electrochem. Soc. 152 (2005) A689–A696.
[31] R. Dedryvere, H. Martinez, S. Leroy, D. Lemordant, F. Bonhomme, P. Biensan, D. Gonbeau, J. Power Sources 174 (2007) 462–468.
[32] H. Tavassol, J.W. Buthker, G.A. Ferguson, L.A. Curtiss, A.A. Gewirth, J. Electrochem. Soc. 159 (2012) A730–A738.
[33] X. Zhang, P.N. Ross, R. Kostecki, F. Kong, S. Sloop, J.B. Kerr, K. Striebel, E.J. Cairns, F. McLarnon, J. Electrochem. Soc. 148 (2001) A463–A470.
[34] A. Aoki, Jpn. J. Appl. Phys. 15 (1976) 305–311.
[35] J.C. Carver, T.A. Carlson, Gk Schweitz, J. Chem. Phys. 57 (1972) 973–982.
[36] J. Yuan, J. Zhu, H. Bi, Z. Zhang, S. Chen, S. Liang, X. Wang, RSC Adv. 3 (2013) 4400–4407.
[37] A. Lebugle, U. Axelsson, R. Nyholm, N. Martensson, Phys. Scr. 23 (1981) 825–827.
[38] M. Oku, K. Hirokawa, S. Ikeda, J. Electron, Spectrosc. Relat. Phenom. 7 (1975) 465–473.
[39] C.S. Fadley, D.A. Shirley, A.J. Freeman, P.S. Bagus, J.V. Mallow, Phys. Rev. Lett. 23 (1969) 1397.
[40] V. Dicastro, G. Polzonetti, J. Electron, Spectrosc. Relat. Phenom. 48 (1989) 117–123.
[41] O.K. Park, Y. Cho, S. Lee, H.C. Yoo, H.-K. Song, J. Cho, Energy Environ. Sci. 4 (2011) 1621–1633.
[42] O.W. Duckworth, S.T. Martin, Geochim. Cosmochim. Acta 68 (2004) 607–621.
[43] Y. Lai, Z. Cao, H. Song, Z. Zhang, X. Chen, H. Lu, M. Jia, J. Li, J. Electrochem. Soc. 159 (2012) A1961–A1966.